Effect of biosurfactant as a novel draw solution on photocatalytic treatment and desalination of produced water by different forward osmosis membranes

Maryam Taghizadeh, Daryoush Yousefi Kebria and Farhad Qaderi

ABSTRACT

Water stress and environmental concerns have driven research into the treatment of produced water. In this study, a combination of forward osmosis and photocatalyst system was used for simultaneous salt removal and treatment of produced water. Furthermore, biosurfactant as a novel draw solution and the three types of forward osmosis membranes (cellulose triacetate with and without titanium dioxide (TiO_2) and graphene oxide (GO) nanoparticles) were investigated. The morphology and distribution of the TiO_2 and TiO_2/GO on the membrane surface were assessed by various analyses including field emission scanning electron microscopy, energy dispersive X-ray and contact angle analysis. The results demonstrated that the reverse salt flux was only 0.2 g/m^2 h. Moreover, benzene, toluene, ethylbenzene, and xylene (BTEX) removal efficiency in the cellulose triacetate with TiO_2 and TiO_2/GO membrane under UVC radiation was 62% and 78%, respectively, while the data obtained in visible light reached 80%. The use of TiO_2 and TiO_2/GO membranes significantly improved the permeability, water flux, photocatalytic degradation of pollutants and desalination of produced water.

Key words | brine, BTEX decomposition, desalination, forward osmosis, graphene oxide, TiO_2

Maryam Taghizadeh
Daryoush Yousefi Kebria (corresponding author)
Farhad Qaderi
Environmental Department of Civil Engineering Faculty,
Babol University of Technology,
P.O. Box: 484, 00981132331707, Babol,
Iran
E-mail: *dy.kebria@nit.ac.ir*

INTRODUCTION

Oil and gas production is usually accompanied by the production of much water. The ratio of produced water to the oil may change from seven to ten times over the lifetime of any oil fields. The produced water is composed of various harmful compounds such as benzene, toluene, ethylbenzene, and xylenes (BTEX) (Dórea *et al.* 2007; Xu *et al.* 2013; Abdel-Shafy & Mansour 2016). Similar to other pollutants, BTEX compounds can have adverse impacts on soil and water biology, and cause many health problems (Gao *et al.* 2014; Ebadati *et al.* 2019; Giagnorio *et al.* 2019).

Membrane processes are an effective method to remove various pollutants that have adverse effects on health and the environment from water (Xu *et al.* 2013; Kusworo *et al.* 2019). Although the membrane has many benefits in separating contaminants, the contaminants are not further eliminated. Thus, the combination of a membrane system with other mechanisms of pollution needed to be evaluated. (Grzechulska-Damszel *et al.* 2010; Janus *et al.* 2011; Amini *et al.* 2015; Giagnorio *et al.* 2019).

Forward osmosis (FO) is considered as a versatile system due to lower energy requirements and costs as well as high water recovery. FO is a semi-permeable hydrophilic membrane process which uses osmotic pressure as the driven force for separation of feed and draw solution (Sirinupong *et al.* 2018; Giagnorio *et al.* 2019). Although the application of FO for desalination of produced water has been studied, there is no study on the management of the residues (Fujishima & Zhang 2006; Madaeni & Ghaemi 2007; Vatanpour *et al.* 2011; Vatanpour *et al.* 2012; Niksefat *et al.* 2014; Hegab *et al.* 2016; Zirehpour *et al.* 2016).

An ideal FO membrane has high water permeability, mechanical strength, chemical stability, rejection of solutes,

doi: 10.2166/ws.2019.154

and reduction of internal concentration polarization (ICP). Also, a desirable draw solution must have minimal reverse draw solute flux, high water flux, no toxicity, reasonably low cost, and easy recovery (Ge *et al.* 2013). FO membranes limit the diffusion of ions, but solutes still diffuse through the membrane from the draw solution to the feed solution at a slow rate due to the high concentration difference of ions between the two streams. This phenomenon is known as reverse solute flux. Reverse diffusion from the draw solution to the feed side affects the quality of the feed water, and decreases water flux and increases the cost of replenishing the lost draw solute. Over the past few decades, many efforts have been made to find an appropriate draw solution; for example, monovalent salts have favorable water solubility and they are frequently used. The greatest disadvantage of monovalent salts as a draw solution for FO is their high salt leakage. These draw solutes create high osmotic pressure, but they are costly and their recovery is complex. But biosurfactants have several advantages including lower toxicity and higher biodegradability. They do not need to be recovered and could be used for soil treatment (Nguyen *et al.* 2015).

A photocatalyst can decompose organic contaminants to CO_2 and H_2O under ultraviolet (UV) or visible light without utilizing chemicals. Therefore, the combination of photocatalyst with membrane processes can significantly increase the membrane efficiency (Grzechulska-Damszel *et al.* 2010).

Titanium dioxide (TiO_2) is the most popular photocatalyst for water treatment due to its unique characteristics including high pollution removal efficiency, cost-effectiveness, chemical stability and low toxicity (Grzechulska-Damszel *et al.* 2010; Janus *et al.* 2011). Investigation of membranes with TiO_2 indicated that adding TiO_2 to a membrane led to an increase in membrane flux, contaminant removal and a decrease in fouling (Gao *et al.* 2014; Amini *et al.* 2015).

Li *et al.* investigated the properties and permeation performance of a PES/TiO_2 composite membrane, prepared through the phase inversion method (Li *et al.* 2009). Wu *et al.* have studied the effect of a PES membrane composed of TiO_2/GO. According to their results, TiO_2/GO nanocomposite in the membrane enhanced the hydrophilicity, antifouling ability, thermal stability, and mechanical strength, although the structure of the membrane was not changed (Wu *et al.* 2008).

Graphene oxide (GO) has the highest surface area, of 2,600 m^2/g, and electron mobility among various photocatalysis (Ma *et al.* 2017). Therefore, GO is an ideal nanomaterial to expand the light response of TiO_2 and to improve the efficiency of photocatalysis under both UV and visible light (Zhang *et al.* 2012; Ma *et al.* 2017; Sirinupong *et al.* 2018).

TiO_2/GO is commonly used as a suspended solid in water treatment (Min *et al.* 2012). Although the suspended photocatalyst can more closely come in to contact with contaminants in water and increase catalyst efficiency, separating TiO_2/GO particles from the treated water is very complex and increases the cost of the water treatment. Thus, TiO_2/GO particles can be immobilized on the surface or in the matrix of the water treatment membrane (Gao *et al.* 2013).

Many studies have been carried out on hydrophilicity, fouling, and improvement of the membrane characterization (Gao *et al.* 2013; Xu *et al.* 2013; Gao *et al.* 2014; Sirinupong *et al.* 2018; Kosint & Ratanatamskul 2019). Gao *et al.* investigated the photocatalytic degradation of organic colors under UV light in the UF process, and also, in their other study, evaluated the modified membrane performance under UV and visible light (Gao *et al.* 2013). One of the important inhibitors in desalination of produced water with FO is the existence of contaminant residues in the feed solution after the treatment (Ariono *et al.* 2016). It is assumed that the FO process can adequately reject the pollutants along with activation of TiO_2/GO on the membrane surface, which consequently results in degradation of pollutants without the requirement to separate the photocatalyst.

In this study, a novel draw solution for minimizing the reverse flux of ions during FO desalination by coupling a biosurfactant (Rhamnolipid) to a Na_3PO_4 draw solution was explored. The effect of different concentrations of coupling biosurfactant to a Na_3PO_4, feed solution and three types of membranes on the FO performance (simultaneous salt removal and BTEX decomposition from brine) were investigated. In addition, several parameters including pure water flux, reverse salt flux, NaCl rejection, the morphology and distribution of nanoparticles on the membrane surface (contact angle, SEM and EDX analysis) were evaluated.

MATERIALS AND METHODS

Chemicals and reagents

TiO_2 nanoparticles and sodium chloride (purity, 99%) were obtained from Sigma-Aldrich and Merck-Millipore (Germany), respectively. Three types of membranes (cellulose triacetate (C), cellulose triacetate with TiO_2 nanoparticles (CT), cellulose triacetate with TiO_2 and GO nanoparticles (CT G)) were purchased from Incubator Center at Babol Noshrivani University of Technology. The method of membrane synthesis was described in detail elsewhere (Zirehpour *et al.* 2015).

FO system performance and evaluation of the membranes' transport properties

To investigate the FO membranes' efficiency, water flux and reverse salt flux were determined in a laboratory-scale FO setup (Figure 1). The unit includes two chambers with dimensions of 12 cm length, 8 cm width, and 1 cm depth, giving an effective membrane area of about 96 cm^2 on both sides. The cell was operated with a co-current cross flow. Two diaphragm pumps (Headon, 1.6 LPM) with the same flow (800 ml/min) were used for circulation of the feed and draw solutions. In this study, a NaCl solution (67,139 and 181 g/l) and coupling biosurfactant to a Na_3PO_4 were used as the draw solution. Different concentrations of salinity (35,75 and 100 g/l) and 10 mg/l BTEX was used as feed solution, because the salinity of produced water may range from seawater to that of brine (Neff 2007). The draw solution was prepared using 0.55 M laboratory-grade Na_3PO_4-$12H_2O$ (Merck Co., Ltd, Germany) mixed with 0.5 mM biosurfactant at room temperature for 60 min. These mixtures of phosphate sodium and biosurfactant were then maintained at pH 8 by adding phosphoric acid (H_3PO_4, Merck, 85% purity) and were continually stirred for 24 h before performing FO tests. Also, the FO membranes' fouling was evaluated with protein solution (500 mg/L of BSA (Bovine serum albumin) solution). Filtration experiments were based on the flux decline during BSA filtration. The UVC light was generated by a UV lamp (100 W) with a wavelength below 280 nm (made in Taiwan).

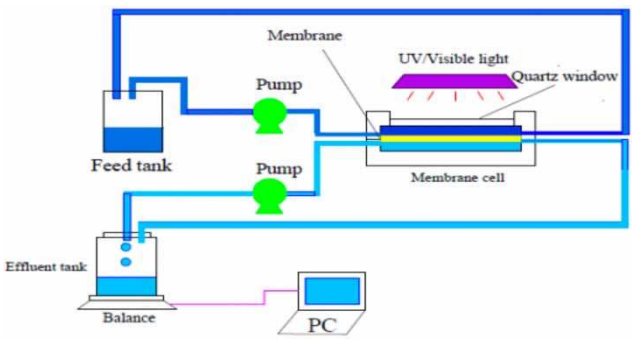

Figure 1 | Schematic diagram of the laboratory-scale cross-flow membrane system.

The FO water flux, J_w, was obtained by using the following equation (Emadzadeh *et al.* 2014):

$$J_w = \frac{\Delta V_{feed}}{A_{membrane} \times \Delta t}$$

where ΔV_{feed} is the volume changes of the feed solution, $A_{membrane}$ is the membrane active surface area and Δt is the evaluating time-interval.

The FO reverse salt flux J_s was determined by calculating the change of salt concentration in the feed solution based on conductivity measurement (Emadzadeh *et al.* 2014):

$$J_s = \frac{V_t \times C_t - V_0 \times C_0}{A_m \times \Delta t}$$

V_t and V_0 are the final and initial volumes of feed solution; C_t and C_0 are the final and initial salt concentrations of the feed solution, respectively.

The pure water permeability (A) and salt permeability (B) of the FO membranes were determined by a cross flow RO unit using 2.5 bar applied pressure. All the membranes were first operated with DI water until the permeate flux became steady (Emadzadeh *et al.* 2014).

Pure water permeability was determined over an applied pressure of 250 kpa with DI water as feed. The A value was calculated according to (Emadzadeh *et al.* 2014):

$$A = \frac{J}{\Delta p}$$

where Δp is the applied pressure and J is the permeation flux.

The salt permeability is determined during RO experiment based on the solution-diffusion theory, as follows (Emadzadeh *et al.* 2014):

$$B = \left(\frac{1-R}{R}\right) \times J$$

where J is the RO permeate flux and the R is the salt rejection of the RO process.

The salt rejection R was evaluated using 20 mM NaCl feed solution. Rejections were determined by conductivity measurement of both the feed and permeate as follows (Emadzadeh *et al.* 2014):

$$R(\%) = \left(1 - \frac{C_p}{C_f}\right) \times 100$$

where C_p and C_f are the salt concentration in the permeate and feed solutions, respectively.

Membrane characterization and BTEX determination

The presence and uniform distribution of the photocatalyst and GO on the three commercial membranes' surfaces ((cellulose triacetate (C), cellulose triacetate with TiO_2 nanoparticles (CT) and cellulose triacetate with TiO_2 and GO nanoparticles (CTG)) were analyzed by field emission scanning electron microscopy (FESEM) and energy dispersive X-ray (EDX). The hydrophilicity of the membrane surface was evaluated by measuring the contact angle with a goniometer (D10, KRUSS, Germany). Also, the amount of aromatic hydrocarbons (BTEX) was analyzed by GC-FID (APHA/AWWA/WEF 1998).

RESULTS AND DISCUSSION

Membrane morphology

FESEM analysis was conducted using a MIRA3TESCAN-XMU microscope in order to confirm the presence of TiO_2 and TiO_2/GO nanoparticles on the surface of all membranes. All of the samples were gold-plated before imaging. The EDX analysis was performed on CT and CTG to ensure the homogeneous dispersion of nanoparticles on the membranes (Figure 2).

These observations confirm the presence of hydrophilic TiO_2 and TiO_2/GO on the top surface of the membrane, since the top of the membrane surface is always exposed

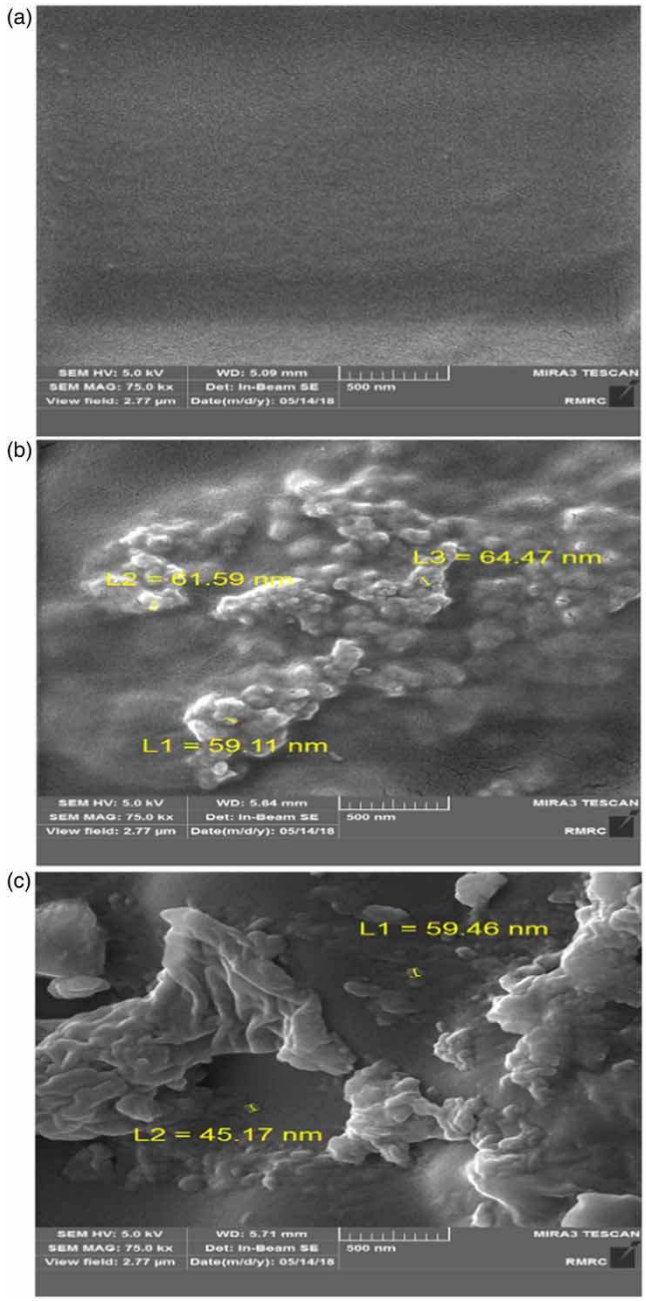

Figure 2 | FESEM images of membrane surfaces: (a) Virgin C (b) CT and (c) CTG (d) EDX result of membrane CT and (e) EDX result of membrane CTG. *(Continued.)*

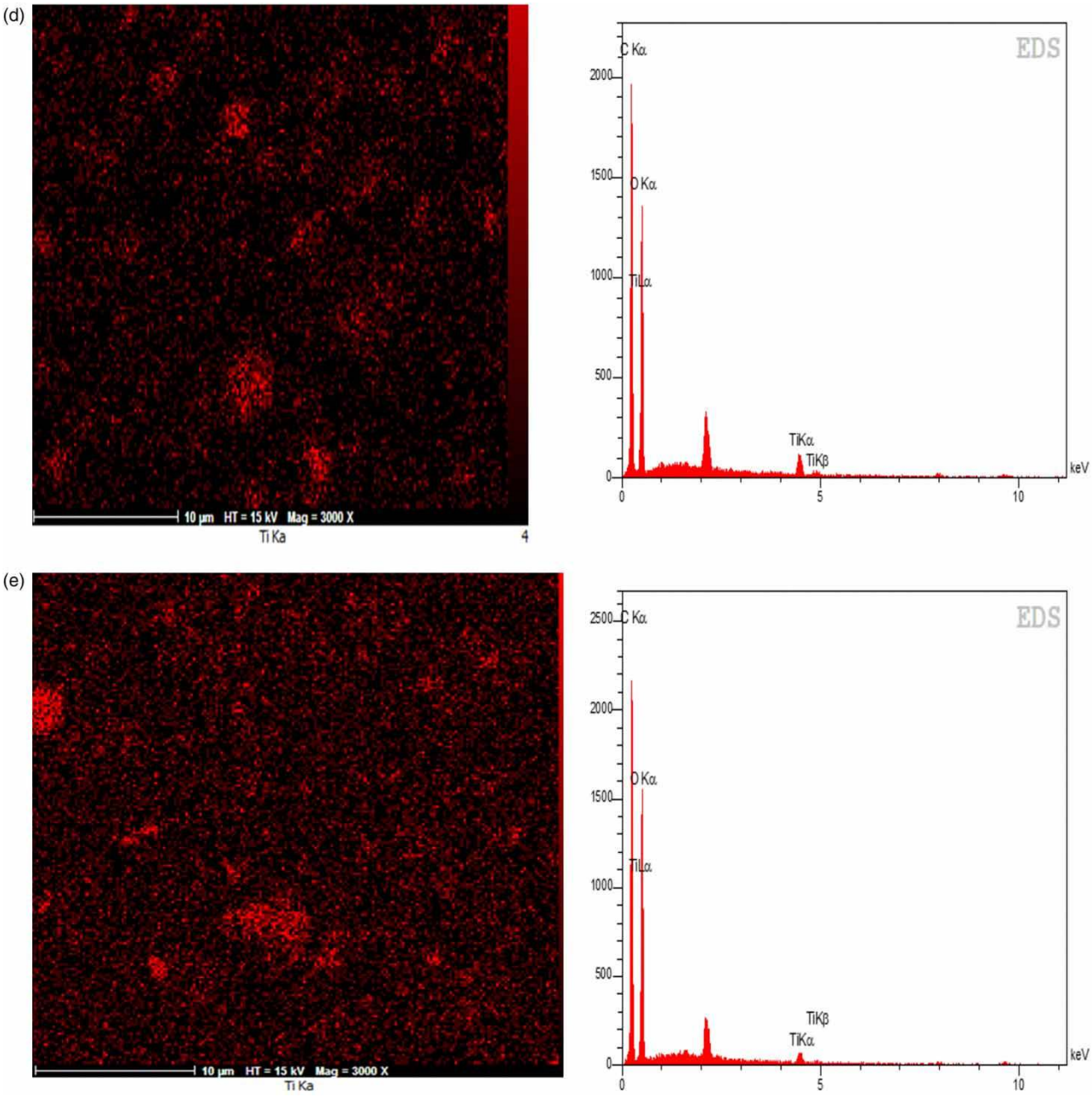

Figure 2 | Continued.

to water. The presence of TiO_2 and TiO_2/GO on the surface of the membrane improves the hydrophilicity of the membrane surface due to hydrophilic functional groups (Zinadini *et al.* 2014; Safarpour *et al.* 2015a, 2015b).

The membrane CT was covered with TiO_2 nanoparticles that accumulated on the surface, while the uniform dispersion of TiO_2 in the TiO_2/GO membrane indicated that the carbon-based structure of GO, TiO_2/GO and CTA polymer and the wimple structure of the GO prevents nanoparticle accumulation and enables their good distribution on the graphene sheets (Gao *et al.* 2013).

Moreover, EDX scanning of the Ti element revealed the uniform dispersion of TiO_2 and TiO_2/GO nanocomposite in the membrane matrix. The red particles in this map are the Ti element of the TiO_2 and TiO_2/GO nanocomposite in the membranes CT and CTG.

The wettability and hydrophilicity of the membrane surface were evaluated using a static contact angle formed between the membrane surface and water (Safarpour *et al.* 2015a, 2015b). Figure 3 illustrates the hydrophilicity of the three membranes (membranes C, CT and CTG).

As shown in Figure 3, the contact angle value of the membrane surface decreased to about 0.1% based on the weight of TiO_2 in CT and about 0.1% based on the weight of TiO_2/GO (ratio 30:70) in the CTG membrane. This decrease is caused by TiO_2/GO hydrophilicity and the presence of the photocatalyst nanoparticles on the membrane surface. The contact angle of the CTG membrane decreased compared to the C and CT membranes because TiO_2/GO nanocomposites have numerous negatively charged oxygen atoms that can increase the surface charge density. This result was confirmed by the FESEM analysis. The high hydrophilicity property of CT and CTG membrane can be related to the higher inclination of TiO_2 to water and hydrolysis with hydroxyl groups.

This matter has also been reported in the other literature (Gao *et al.* 2014; Safarpour *et al.* 2015a, 2015b; Hegab *et al.* 2016).

In order to investigate FO performance, the salt rejection (R), the water permeability coefficient (A) and salt permeability coefficient (B) for all membranes were calculated from the FO experimental data, and the results are summarized in Table 1.

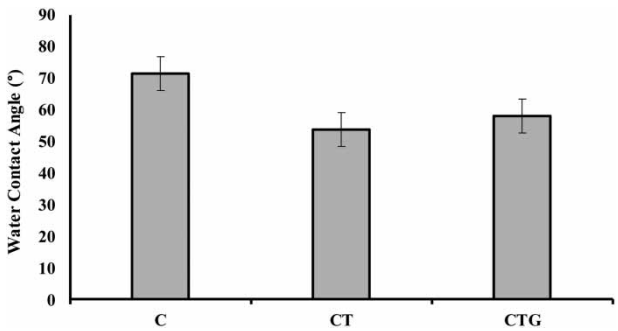

Figure 3 | Water contact angle of all membranes.

Table 1 | Summary of transport parameters R, A, B, and B/A values of all membranes[a]

		Pure water permeability A			
Membrane	**R**	**A (L/m².h.bar)[b]**	**A(m/s.pa)× 10^(−12)**	**B(m/s)× 10^(−8)[c]**	**B/A (Kpa)**
C	85%	0.45 ± 0.04	1.26 ± 0.05	3.4 ± 0.10	26.98
CT	90%	1.64 ± 0.05	4.6 ± 0.10	7.9 ± 0.2	17.17
CTG	89%	1.81 ± 0.05	5.07 ± 0.12	8.7 ± 0.2	17.16

[a]All data are reported as the average of three reported measurements.
[b]RO testing mode, at 2.5 bar pressure, pure water as feed solution.
[c]RO testing mode, 2.5 bar pressure, 20 mM NaCl as feed solution.

The A value in membranes CT and CTG was apparently improved about one to three times compared with membrane C due to the enhancement of hydrophilicity of the membranes.

Also, the presence of TiO_2 and TiO_2/GO on the membrane surface increased parameter B. The salt permeability of the membranes could enhance the rejection ability of the membranes. In this study, the FO membrane had a relatively low salt permeability due to the good rejection ability of the membranes. The B/A ratio is one of the main factors that indicates the selectivity of membranes and consequently leads to the reduction of reverse diffusion released into the feed solution, reduces the fouling tendency, enhances the selectivity, and creates more FO process stabilization during the process. The membranes CT and CTG had a lower B/A value in comparison with membrane C, therefore leading to reverse solution diffusion into the feed solution.

Membrane performance

To evaluate the performance of all membranes, J_w, J_s and normalized flux (J_w/J_{w0}) were measured over 180 minutes (Figure 4). J_w and J_{w0} are the water fluxes during and at the beginning of an experiment.

As can be seen in Figure 4, when the amount of NaCl increased in the feed solution, the normalized flux reduced and this reduction in the CT and CTG membranes was less than in membrane C. Also, the pure water flux increased in the CT and CTG membranes under UV and visible irradiation compared with the C membrane (Figure 5). The high permeability of the CT and CTG membranes might be related to their high hydrophilicity, which is confirmed by contact angle measurement (Figure 3). The increasing

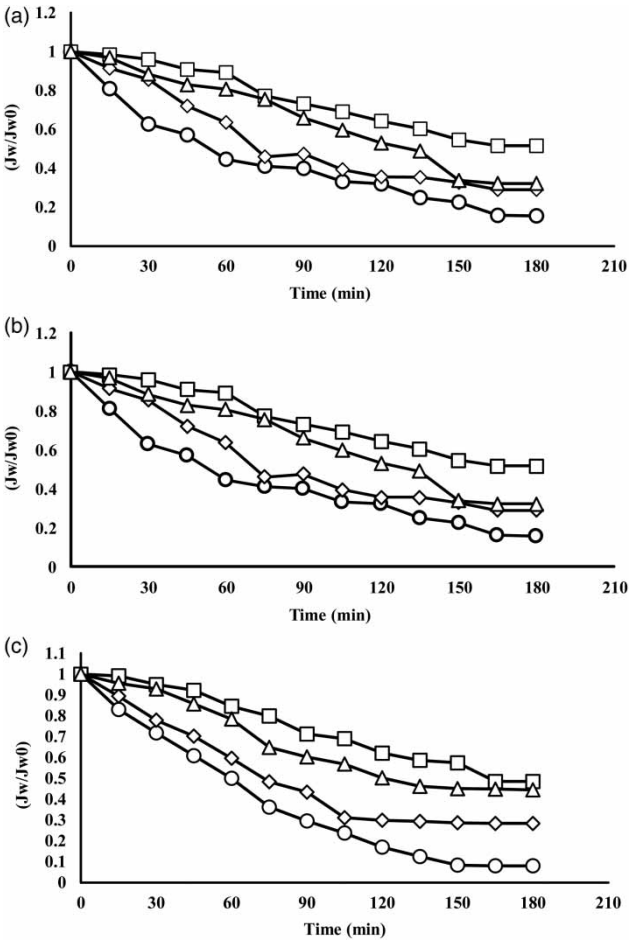

Figure 4 | Normalized flux of the all membranes with different NaCl concentrations and 10 mg/l BTEX as the feed solution, (a) 35 g/l, (b) 75 g/l, (c) 100 g/l.

trend of pure water flux is similar to the decrease in the contact angle. Results in Figure 5 show that coupling a biosurfactant to Na_3PO_4 as the draw solution has higher water flux than NaCl as a draw solution.

When electrons-holes are formed on the surface of TiO_2-GO by UV irradiation, they react with Ti and O_2^- in a different mechanism. The electrons tend to reduce Ti(IV) to Ti(III) and the holes can oxidize O_2^-. The oxygen atoms are separated from the surface and a group of empty sites is produced. These empty sites are occupied with oxygen molecules and adsorb the OH group and increase the surface hydrophilicity (Fujishima & Zhang 2006; Langlet *et al.* 2006; Madaeni & Ghaemi 2007). When the membrane hydrophilicity increases, the water molecules are attracted inside the membrane matrix and subsequently the water permeability of the membrane increases. Although the CT membrane has the highest hydrophilicity, it has the lowest pure water flux due to the TiO_2 nanoparticles' tendency to accumulate because of its carbon-based nanomaterials (as shown in Figures 4 and 5). TiO_2 has a high specific surface area and the hydroxyl groups on its surface can accumulate and form large size TiO_2, which consequently could block the membrane pores and reduce the pure water flux (Wei *et al.* 2011; Zhao *et al.* 2013).

According to Figure 5, the flux of the membrane under UV light was greater than in visible light, because the visible light is less effective than UV in increasing membrane hydrophilicity (Gao *et al.* 2014).

The reverse salt flux was measured when NaCl and biosurfactant were coupled to Na_3PO_4 as a draw solution with deionized (DI) water as a feed solution. According to the solution-diffusion theory, the solute flux is inversely related to the salt rejection coefficient (R). The higher rejection led to lower solute flux (Niksefat *et al.* 2014; Amini *et al.* 2015; Zirehpour *et al.* 2015, 2016). Based on Table 1, the rejection coefficient (R) of CT and CTG membranes was greater than that of the C membrane, therefore the reverse salt flux decreased (Figure 5). (Vatanpour *et al.* 2011, 2012; Zhang *et al.* 2012; Gao *et al.* 2014). In Figure 5, the reverse salt flux decreased when a biosurfactant was coupled to Na_3PO_4 as a draw solution. When the pH value of the draw solution was fixed at pH 8, the main ion composition was Na^+, $NaHPO_4^-$ and HPO_4^{2-} and the FO membrane exhibited a negative charge (Nguyen *et al.* 2015). Therefore, Na^+ with positive charge may easily pass through the FO membrane because of the electrostatic attraction. It is assumed that when the biosurfactant was coupled to Na_3PO_4, between tail groups of biosurfactant with membrane hydrophobic interactions occur and an additional layer was formed on the membrane surface. This layer prevented ions from exiting through the membrane pores, and therefore reduced the reverse salt flux. This phenomenon is in agreement with other studies. However, water flux decreased when the concentration of biosurfactant increased because the internal concentration polarization and viscosity of the draw solution increased, thus the diffusivity of water through the FO membrane changed, as shown in Figure 5 (Nguyen *et al.* 2015).

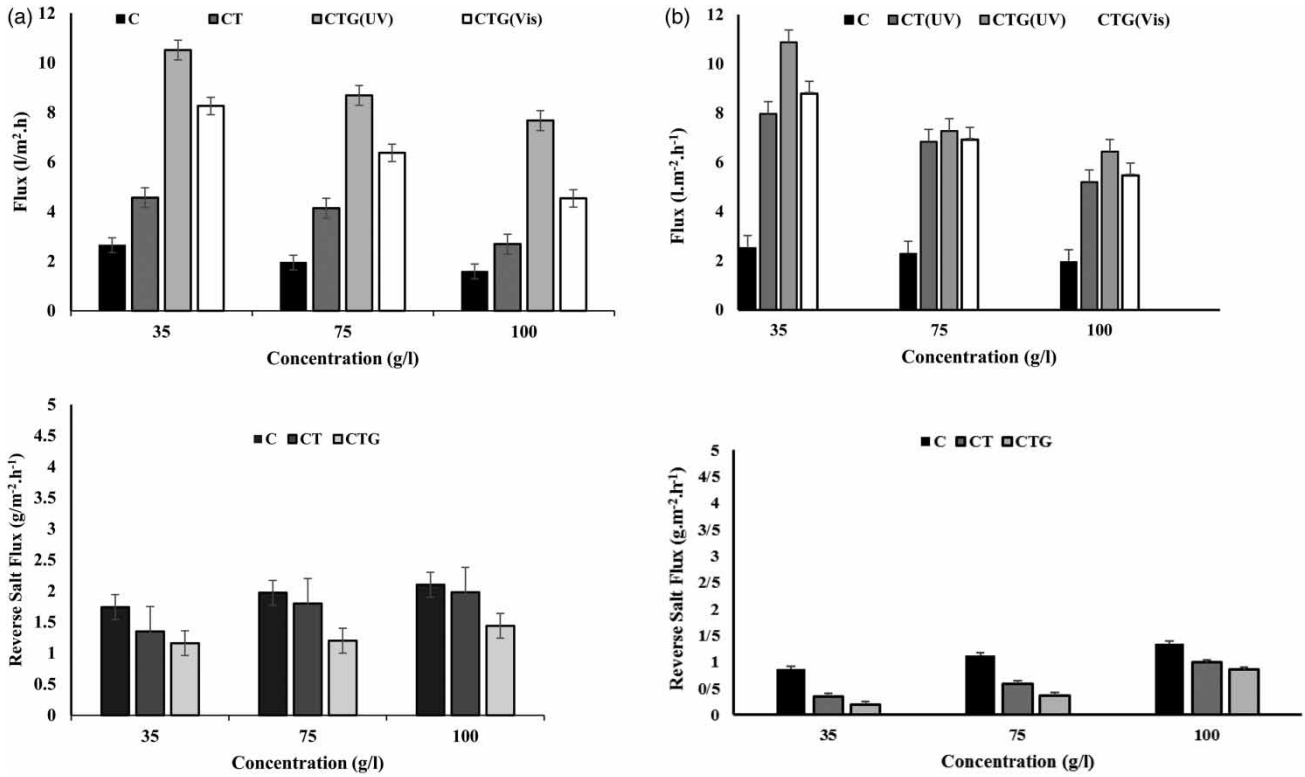

Figure 5 | Water flux and J_s of all membranes with different NaCl concentration and 10 mg/l BTEX as the feed solution: (a) NaCl as a draw solution, (b) biosurfactant coupled to Na_3PO_4 as a draw solution.

Antifouling performance of FO membrane

The fouling evaluation of the FO membranes was performed using a 500 mg/L BSA solution (Figure 6). According to the water flux decline of the membranes, the virgin C membrane has the highest loss of water flux compared to the CT and CTG membranes. The water flux of virgin C membrane declined to 45% of its initial value after 180 min filtration of BSA solution. In contrast, the CT and CTG membrane preserves around 75% and 80% of its initial flux. The high fouling resistance of the CT and CTG membranes was due to their favorable hydrophilicity and negative charge. The fouling agents have a negative surface charge. Therefore, due to the negative charge of the membrane surface, as shown in previous studies, the biofilm formation decreased (Safarpour *et al.* 2015a, 2015b).

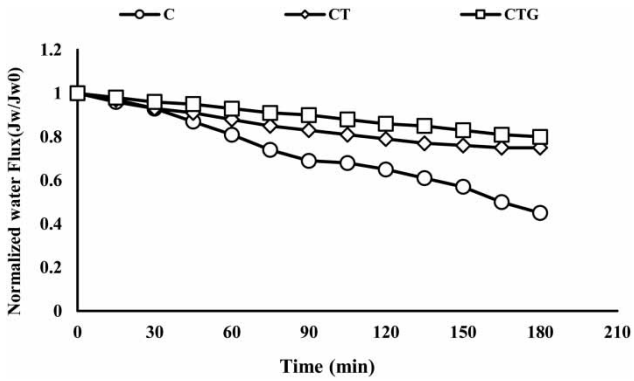

Figure 6 | Normalized water flux of the FO membranes during filtration of 500 mg/L BSA solution.

Photocatalytic performance

The pure water flux of the CT and CTG membranes with three different feed solution concentrations was analyzed in a cross-flow membrane filtration system with a windowed membrane cell. The window allows a tested membrane to be exposed to light irradiation (Figure 7).

One of the main challenges in produced water treatment with the FO process is the high concentration of BTEX in

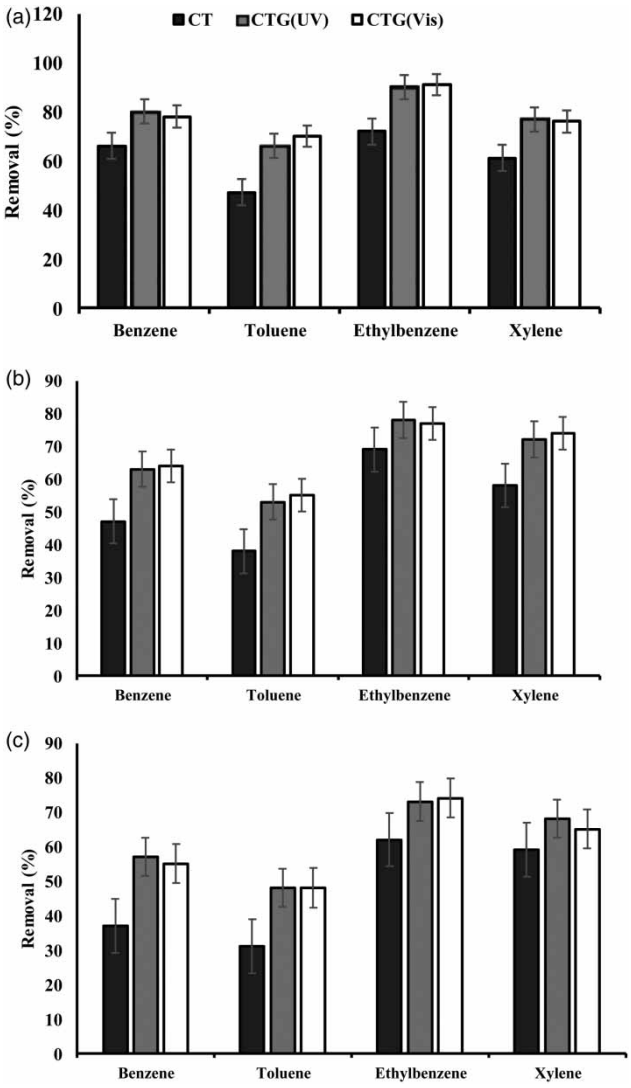

Figure 7 | BTEX compounds' removal efficiency by membranes CT and CTG with different NaCl concentrations and 10 mg/l BTEX as the feed solution: (a) 35 g/l, (b) 75 g/l, and (c) 100 g/l (after 180 min at T = 25°).

the effluent. Figure 7 illustrates the removal efficiency of BTEX in photoactivity under UV and visible light (Gao *et al.* 2014).

When the light intensities are equal to or greater than the band gap energy that irradiated a semiconductor object in normal conditions, an electron is transferred from the capacity band to the conduction band, so a pair of holes-electron are created on the surface of the semiconductor object (Langlet *et al.* 2006; Madaeni & Ghaemi 2007).

UV irradiation causes formation of the electron-hole on the surface because TiO_2/GO is a semiconductor. These electrons react with the oxygen molecules in the water and produce O_2^-, and the holes react with the water and produce the OH radical. The O_2^- and OH radical are strong oxidant reagents and can decompose BTEX from water (Mills *et al.* 2002; Guan 2005).

As shown in Figure 7, the BTEX photodegradation efficiency of the membrane CTG under UV was relatively equal to visible light and better than that of achieved by CT membrane results. This result confirms that TiO_2 with GO decreases the band-gap energy of each semiconductor so that these semiconductors can be active under visible light and hence leads to photocatalytic activities. Also, the efficiency of ethylbenzene degradation was slightly higher than that for the other BTEX components (Gao *et al.* 2014).

CONCLUSION

This study showed that a co-FO system with photocatalyst exhibited significant ability in desalination and reducing residues of produced water, simultaneously. According to the results from the laboratory scale, FO tests suggest that coupling a biosurfactant to the Na_3PO_4 draw solution could reduce reverse salt flux. Compared with traditional draw solutes for FO (0.22–2.48 g), the draw solute of Na_3PO_4 coupled with biosurfactant in this study exhibited less loss (approximately 0.2 g) per liter of water recovered. The result for CT and CTG membranes in comparison with the C membrane showed that the presence of TiO_2 and GO nanoparticles improved the permeability, increased hydrophilicity and enhanced the FO efficiency. This observation confirms that combining TiO_2 with GO activates electrons and leads to photocatalytic activities under both UV and visible light with a decrease in the band-gap energy. The best BTEX removal efficiency obtained was 80% in membrane CTG under visible light.

REFERENCES

Abdel-Shafy Hussein, I. & Mansour, S. M. 2016 A review on polycyclic aromatic hydrocarbons: source, environmental impact, effect on human health and remediation. *Egyptian Journal of Petroleum* **25** (1), 107–123.

Amini, M., Rahimpour, A. & Jahanshahi, M. 2015 Forward osmosis application of modified TiO_2-polyamide thin film nanocomposite membranes. *Desalination and Water Treatment* **57** (30), 14013–14023.

APHA/AWWA/WEF 1998 *Standard Methods for the Examination of Water and Wastewater*, 20th edn. American Public Health Association/American Water Works Association/Water Envitonmental Federation, Washington, DC, USA.

Ariono, D., Purwasasmita, M. R. & Wenten, I. G. 2016 Brine effluents: characteristics, environmental impacts, and their handling. *Journal of Engineering and Technological Sciences* **48** (4), 367–387.

Dórea, H. S., Bispo, J., Aragão, K. A. S., Cunha, B., Navickiene, S., Alves, J., Romão, L. & Garcia, C. 2007 Analysis of BTEX, PAHs and metals in the oilfield produced water in the state of Sergipe, Brazil. *Microchemica Journal* **85** (2), 234–238.

Ebadati, A., Davarpanah, A., Shahhoseini, A. & Ahmadi, P. 2019 An experimental study to measure the required fresh water and treated water for drilling an unconventional shale reservoir. *International Journal of Environmental Science and Technology* **16**, 7727–7734.

Emadzadeh, D., Lau, W. J., Matsuura, T., Rahbari-Sisakht, M. & Ismail, A. F. 2014 A novel thin film composite forward osmosis membrane prepared from PSf-TiO_2 nanocomposite substrate for water desalination. *Chemical Engineering Journal* **237**, 70–80.

Fujishima, A. & Zhang, X. 2006 Titanium dioxide photocatalysis: present situation and future approaches. *Comptes Rendus Chimie* **9** (5–6), 750–760.

Gao, P., Liu, Z., Tai, M., Sun, D. & Ng, W. 2013 Multifunctional graphene oxide-TiO_2 microsphere hierarchical membrane for clean water production. *Applied Catalysis B: Environmental* **138–139**, 17–25.

Gao, Y., Hu, M. & Mi, B. 2014 Membrane surface modification with TiO_2 – graphene oxide for enhanced photocatalytic performance. *Journal of Membrane Science* **455**, 349–356.

Ge, Q., Ling, M. & Chung, T. 2013 Draw solutions for forward osmosis processes: developments, challenges, and prospects for the future. *Journal of Membrane Science* **442**, 225–237.

Giagnorio, M., Ricceri, F. & Tiraferri, A. 2019 Desalination of brackish groundwater and reuse of wastewater by forward osmosis coupled with nanofiltration for draw solution recovery. *Water Research* **153**, 134–143.

Grzechulska-Damszel, J., Mozia, S. & Morawski, A. W. 2010 Integration of photocatalysis with membrane processes for purification of water contaminated with organic dyes. *Catalysis Today* **156** (3–4), 295–300.

Guan, K. 2005 Relationship between photocatalytic activity, hydrophilicity and self-cleaning effect of TiO_2/SiO_2 films. *Surface and Coatings Technology* **191** (2–3), 155–160.

Hegab, H. M., ElMekawy, A., Barclay, T. G., Michelmore, A., Zou, L., Saint, C. P. & Markovic, M. 2016 Effective *in-situ* chemical surface modification of forward osmosis membranes with polydopamine-induced graphene oxide for biofouling mitigation. *Desalination* **385**, 126–137.

Janus, M., Kusiak-Nejman, E. & Morawski, A. W. 2011 Determination of the photocatalytic activity of TiO_2 with high adsorption capacity. *Reaction Kinetics, Mechanisms and Catalysis* **103** (2), 279–288.

Kosint, K. & Ratanatamskul, C. 2019 TiO_2-nanoparticles coated forward osmosis membranes for enhanced filtration of textile effluent. *IOP Conference Series: Earth and Environmental Science* **219** (1).

Kusworo, T. D., Aryanti, N., Utomo, Q. & Widayat, D. P. 2019 Improvement in nano-hybrid membrane PES–nanosilica performance using ultra violet irradiation and acetone–ethanol immersion for produced water treatment. *International Journal of Environmental Science and Technology* **16** (2), 973–986.

Langlet, M., Permpoon, S., Riassetto, D., Berthomé, G., Pernot, E. & Joud, J. C. 2006 Photocatalytic activity and photo-induced superhydrophilicity of Sol-Gel derived TiO_2 films. *Journal of Photochemistry and Photobiology A: Chemistry* **181** (2–3), 203–214.

Li, J., Xu, Z., Yang, H., Li, Y. & Liu, M. 2009 Effect of TiO_2 nanoparticles on the surface morphology and performance of microporous PES membrane. *Applied Surface Science* **255** (9), 4725–4732.

Ma, J., Ping, D. & Dong, X. 2017 Recent developments of graphene oxide-based membranes: a review. *Membranes* **7** (3).

Madaeni, S. S. & Ghaemi, N. 2007 Characterization of self-cleaning RO membranes coated with TiO_2 particles under UV irradiation. *Journal of Membrane Science* **303** (1–2), 221–233.

Mills, A., Elliott, N., Parkin, I., O'Neill, S. A. & Clark, R. J. 2002 Novel TiO_2 CVD films for semiconductor photocatalysis. *Journal of Photochemistry and Photobiology A: Chemistry* **151** (1–3), 171–179.

Min, Y., Zhang, K., Zhao, W., Zheng, F., Chen, Y. & Zhang, Y. 2012 Enhanced chemical interaction between TiO_2 and graphene oxide for photocatalytic decolorization of methylene blue. *Chemical Engineering Journal* **193–194**, 203–210.

Neff, J. M. 2007 *Produced Water. Bioaccumulation in Marine Organisms*, 1st edn. Elsevier Science, Amsterdam, The Netherlands. doi:10.1016/b978-008043716-3/50002-6.

Nguyen, H., Nguyen, C., Chen, S., Li, C., Hsu, H. & Wu, S. 2015 Innovation in draw solute for practical zero salt reverse in forward osmosis desalination. *Industrial & Engineering Chemistry Research* **54** (23), 6067–6074.

Niksefat, N., Jahanshahi, M. & Rahimpour, A. 2014 The effect of SiO_2 nanoparticles on morphology and performance of thin film composite membranes for forward osmosis application. *Desalination* **343**, 140–146.

Safarpour, M., Khataee, A. & Vatanpour, V. 2015a Effect of reduced graphene oxide/TiO_2 nanocomposite with different molar ratios on the performance of PVDF ultrafiltration membranes. *Separation and Purification Technology* **140**, 32–42.

Safarpour, M., Vatanpour, V. & Khataee, A. 2015b Preparation and characterization of graphene oxide/TiO_2 blended PES nano

Filtration membrane with improved antifouling and separation performance. *Desalination* **393**, 65–78.

Sirinupong, T., Youravong, W., Tirawat, D., Lau, W. J., Lai, G. S. & Ismail, A. F. 2018 Synthesis and characterization of thin film composite membranes made of PSF-TiO_2/GO nanocomposite substrate for forward osmosis applications. *Arabian Journal of Chemistry*. King Saud University.

Vatanpour, V., Madaeni, S., Moradian, R., Zinadini, S. & Astinchap, B. 2011 Fabrication and characterization of novel antifouling nanofiltration membrane prepared from oxidized multiwalled carbon nanotube/polyethersulfone nanocomposite. *Journal of Membrane Science* **375** (1–2), 284–294.

Vatanpour, V., Madaeni, S., Khataee, A., Salehi, E., Zinadini, S. & Ahmadi Monfared, H. 2012 TiO_2 embedded mixed matrix PES nanocomposite membranes: influence of different sizes and types of nanoparticles on antifouling and performance. *Desalination* **292**, 19–29.

Wei, Y., Chu, H., Dong, B., Li, X., Xia, S. & Qiang, Z. 2011 Effect of TiO_2 nanowire addition on PVDF ultrafiltration membrane performance. *Desalination* **272** (1–3), 90–97.

Wu, G., Gan, S., Cui, L. & Xu, Y. 2008 Preparation and characterization of PES/TiO_2 composite membranes. *Applied Surface Science* **254** (21), 7080–7086.

Xu, C., Cui, A., Xu, Y. & Fu, X. 2013 Graphene oxide-TiO_2 composite filtration membranes and their potential application for water purification. *Carbon* 465–471.

Zhang, Y., Zhang, N., Tang, Z. & Xu, Y. 2012 Improving the photocatalytic performance of graphene-TiO_2 nanocomposites via a combined strategy of decreasing defects of graphene and increasing interfacial contact. *Physical Chemistry Chemical Physics* **14** (25), 9167–9175.

Zhao, C., Xu, X., Chen, J. & Yang, F. 2013 Effect of graphene oxide concentration on the morphologies and antifouling properties of PVDF ultrafiltration membranes. *Journal of Environmental Chemical Engineering* **1** (3), 349–354.

Zinadini, S., Zinatizadeh, A., Rahimi, M., Vatanpour, V. & Zangeneh, H. 2014 Preparation of a novel antifouling mixed matrix PES membrane by embedding graphene oxide nanoplates. *Journal of Membrane Science* **453**, 292–301.

Zirehpour, A., Rahimpour, A., Seyedpour, F. & Jahanshahi, M. 2015 Developing new CTA/CA-based membrane containing hydrophilic nanoparticles to enhance the forward osmosis desalination. *Desalination* **371**, 46–57.

Zirehpour, A., Rahimpour, A., Khoshhal, S., Dadashi Firouzjaei, M. & Ghoreyshi, A. 2016 The impact of MOF feasibility to improve the desalination performance and antifouling properties of FO membranes. *RSC Advances* **6** (74), 70174–70185.

First received 24 July 2019; accepted in revised form 13 October 2019. Available online 30 October 2019